Preparation of active films with enhanced antioxidant and antibacterial properties by incorporating ginger essential oil nanoemulsions with xylan and PVA

Junhan Liu [a, b], Marie-Laure Fauconnier [b], Aurore Richel [c], Yuhong Jin [a, *]

[a] Key Laboratory of Food Processing Technology and Quality Control in Shandong Province, College of Food Science and Engineering, Shandong Agricultural University, Tai'an 271018, China.

[b] Laboratory of Chemistry of Natural Molecules, Gembloux Agro-Bio Tech, University of Liége, Passage des déportés 2, B-5030, Gembloux, Belgium.

[c] Laboratory of Biomass and Green Technologies, Gembloux Agro-Bio Tech, University of Liege, Passage des déportés 2, B-5030, Gembloux, Belgium.

*Corresponding author: yuhongjin79@sdau.edu.cn

Abstract

In this study, active films were successfully prepared using xylan/polyvinyl alcohol (PVA) as the film-forming matrix, combined with ginger essential oil nanoemulsions (GEO-NEs) at varying concentrations (2.0%, 4.0%, 6.0%, and 8.0% w/w). The GEO-NEs, produced via ultrasound, had an average particle size of 176.4±1.2 nm. FTIR and XRD analyses revealed that interactions between GEO-NEs and the film matrix occurred through hydrogen bonding, indicating good compatibility between the components. Incorporating GEO-NEs significantly enhanced the UV shielding performance and mechanical properties of the composite films, achieving mechanical properties comparable to those of commercial packaging materials such as high-density polyethylene (HDPE). The GEO-NEs also boosted the antioxidant and antimicrobial activities of the films, producing inhibition zones against Staphylococcus aureus and Escherichia coli. These results suggest that the composite films have excellent UV shielding, mechanical properties, as well as antioxidant and antibacterial activities, indicating their potential application as active food packaging materials.

Keywords

Ginger essential oil, Nanoemulsions, Xylan, Polyvinyl alcohol, Active films

1. Introduction

As conventional plastic production continues to deplete petroleum resources, significant attention has shifted towards novel packaging materials derived from biopolymers such as polysaccharides, proteins, and lipids. These biopolymers offer advantages such as non-toxicity, biodegradability, renewability, and edibility, thereby presenting broad prospects for various applications (Chen et al., 2024; Jurić, Maslov Bandić, Carullo, & Jurić, 2024).

Xylan is a primary component of plant hemicellulose, characterized by a backbone composed of β-(1,4)-linked D-xylopyranosyl residues. It is widely distributed in nature and plentiful in dicots, grasses, and gymnosperms, making it the second most abundant renewable plant polysaccharide on Earth after cellulose (Curry, Peña, & Urbanowicz, 2023; Ye & Zhong, 2022). However, xylan main chains contain numerous hydroxyl groups, leading to the formation of dense hydrogen bonding structures during the film formation process. This results in defects such as brittleness and hygroscopicity in pure xylan films, which are unsuitable for food packaging (Höije, Gröndahl, Tømmeraas, & Gatenholm, 2005; Sárossy et al., 2013). To address these issues, researchers have modified the structure of xylan (Mikkonen et al., 2015; Rao et al., 2021; Šimkovic et al., 2014; Zhang, Li, Qi, & Xiang, 2024) or blended xylan/modified xylan with plasticizers and other polymers to enhance the properties of pure xylan films (Bao et al., 2018; Liu et al., 2019b; Sousa, Ramos, Evtuguin, & Gamelas, 2016; Wang et al., 2022; Wang et al., 2021). Polyvinyl alcohol (PVA) is a widely used, non-toxic, water-soluble polymer known for its excellent chemical stability, biocompatibility, and biodegradability, making it highly promising for food packaging applications (Oun, Shin, Rhim, & Kim, 2022). Previous studies have shown that composite films made by blending xylan with PVA exhibit good compatibility and mechanical properties (Liu et al., 2019b; Wang et al., 2014). However, the antioxidant and antibacterial activities of xylan/PVA films are relatively weak or absent, posing a challenge for extending the shelf life of food products.

Ginger essential oil (GEO), derived from the rhizomes of ginger (*Zingiber officinale Roscoe*), contains an array of compounds including α-zingiberene, geranial, β-

sesquiphyllandrene, α-curcumene, and β-bisabolene. These compounds impart GEO with its distinctive aroma and confer antimicrobial and antioxidant activities (He et al., 2023). Essential oils (EOs) have been classified as Generally Recognized as Safe (GRAS) by the U.S. Food and Drug Administration as natural preservatives (Pandey, Islam, Shams, & Dar, 2022). However, EOs typically exhibit strong taste, high volatility, and low water solubility, which limits their effective application in food packaging (Lakshmayya et al., 2023). An effective strategy to overcome these limitations is to encapsulate EOs into oil-in-water nanoemulsions, creating essential oil-based nanoemulsions (EO-NEs). This approach helps mask the strong aroma of EOs and enhances their compatibility with various biopolymer matrixes (Mirsharifi, Sami, Jazaeri, & Rezaei, 2023). EO-NEs can be prepared using high-energy emulsification techniques such as high-pressure homogenization, ultrasonication, and microfluidization, yielding droplets with an average size ranging from 20 to 200 nm (Singh & Pulikkal, 2022). Research indicates that EO-NEs not only effectively preserve the bioactive constituents of EOs but also exhibit superior antibacterial activity (Shi, Zhang, Chen, & Wang, 2022). In recent years, researchers have attempted to incorporate EO-NEs into various biopolymer-based films such as gelatin (Li et al., 2020; Sun et al., 2021), chitosan (Rui et al., 2024), sodium alginate (Mutlu, 2023), pectin (Norcino et al., 2020), starch (Fan et al., 2024; Kong et al., 2020; Sanchez, Pinzon, & Villa, 2022), and zein (Li et al., 2022). Furthermore, the results indicate good compatibility between these biopolymers and EO-NEs.

To our knowledge, no studies have been reported on xylan/PVA films containing GEO-NEs. The primary objective of this study was to develop active films based on xylan/PVA with enhanced antioxidative and antibacterial properties (Fig. 1). Furthermore, the influence of different concentrations of GEO-NEs on the physicochemical, antioxidative, and antibacterial properties of the films was examined to evaluate the potential application of xylan/PVA-based active films in food preservation.

2. Materials and methods

2.1. Materials

Xylan derived from corn cobs was purchased from Aladdin Reagent Co., Ltd. (Shanghai, China). Polyvinyl alcohol, glycerol, and Tween 80 were obtained from Sinopharm Chemical Reagent Co., Ltd. (Shanghai, China). Ginger essential oil was supplied by Huashuo Spice Oil Co., Ltd. (Jiangxi, China). Mueller Hinton agar was purchased from Weiju Biotechnology Co., Ltd. (Nanjing, China). *Escherichia coli* ATCC 25922 and *Staphylococcus aureus* ATCC 6538 were deposited in the College of Food Science and Engineering, Shandong Agricultural University. All other reagents were of analytical grade.

2.2. Preparation and characterization of nano-emulsions

According to the method of Li et al. (2023), with slight modifications, the crude emulsion was obtained by mixing a 1% Tween-80 solution with 2 g of ginger essential oil and shearing at 20,000 × g for 5 min using a high-speed shear (T18 digital Ultra-Turrax, IKA, Germany). The nanoemulsion was then produced using an ultrasonic cell crusher (VCX 130, SONICS, USA) with a 10-min ultrasonic crushing time, a 3-sec ultrasonic crushing interval, and an ultrasonic crushing power of 130 W.

The particle size, polydispersity index (PDI), and zeta potential of GEO-NEs were determined at 25°C using a nanoparticle size and potential analyzer (NS-90Z, OMEC, China). To reduce the multiple light scattering effect, the GEO-NEs were diluted 100 times with deionized water and left for 1 minute before testing (Shi et al., 2022). Additionally, the average particle size, PDI, and zeta potential of GEO-NEs were recorded at 7, 14, 21, and 28 d to assess the stability of GEO-NEs. The GEO-NEs were also observed at 40× magnification using an inverted fluorescence microscope (MF53-N, MSHOT, China)

2.3. Preparation of films

The composite films were prepared using the solution casting method, based on the procedure outlined by Wang et al. (2014), with slight modifications.

Briefly, 1.5 g of PVA particles were dissolved in 90 mL of deionized water and stirred at 95°C until the PVA formed a homogeneous solution. Once cooled to 80°C, 0.5 g of xylan was added to the PVA solution and stirred for 30 min. After further cooling to 40°C, 20% glycerol (based on the total weight of PVA and xylan) was added and stirred for an additional 30 min to obtain a film-forming solution (FFS). GEO-NEs (at concentrations of 2%, 4%, 6%, and 8% of the total film volume) were added to the FFS and stirred for 20 min at room temperature to obtain active FFS, labeled as GEO-NEs 2%, 4%, 6%, and 8%, respectively. After stationary defoaming, 25 g of the resulting active FFS was cast onto polystyrene molds (10 cm × 10 cm) and dried in an oven at 40°C for 6 to 8 h. All films were conditioned at 23°C and 50% RH for 48 h before analysis.

2.4. Characterization of active films

2.4.1. Attenuated total reflectance–Fourier transform infrared (ATR–FTIR)

The ATR-FTIR spectra of the films were recorded using a Nicolet iS10 FTIR spectrometer (Thermo Fisher Scientific, USA). The absorption spectra were collected in the wavenumber range of 4000 to 400 cm^{-1} with a scan rate of 32 scans and a resolution of 4 cm^{-1}.

2.4.2. Scanning electron microscopy (SEM) observation

The morphology characteristics of the film surface and cross-section were observed using a field emission scanning electron microscope (SEM, JSM-7800F, JEOL Ltd., Tokyo, Japan). To observe the cross-section, the film was immersed in liquid nitrogen for 5 min and then fractured. All samples were sputter-coated with gold for 50 sec at a current of 15 mA to make them conductive, followed by observation at magnifications of 500× and 1000×.

2.4.3. X-ray diffraction test (XRD)

The crystallinity of the films was evaluated using an X-ray diffractometer (D8 ADVANCE, Bruker, Germany). Samples were scanned at diffraction angles (2θ)

between 5° and 80° at a scanning rate of 5°/min.

2.4.4. Optical properties

The white standard plate (L*=92.7, a*=1.01, b*=0.64) was used as the background, and the L (lightness), a (redness), and b (yellowness) values were determined by using a colorimeter (CR-400, Konica Minolta Co., Ltd., Japan) to take samples from six random positions of each film. The total color difference (ΔE) was calculated by the following equation:

$$\Delta E = \sqrt{(L^* - L)^2 + (a^* - a)^2 + (b^* - b)^2}$$

where L*, a*, b* are the color values of the white standard plate, L, a, b were the color values of film samples.

The UV-visible transmittance of the films was recorded using a UV-visible spectrophotometer (UV-2600i, Shimadzu, Japan) in the wavelength range of 200-800 nm. The opacity of the films was determined according to the following equation:

$$Opacity = \frac{A_{600}}{X}$$

where A_{600} is the absorbance at 600 nm and X is the film thickness (mm).

2.4.5. Thickness and mechanical properties

Film thickness was measured using a digital micrometer caliper (Sanfeng Precision Meter Co., Ltd., Shanghai, China) at twelve random positions on the film. The tensile strength (TS) and elongation at break (EB) of the films were determined using an auto tensile tester (Labthink Instruments Co. Ltd., Jinan, China) based on a previous method by Qin, Yang, Zhu, and Wei (2022). Before analysis, films were cut into strips measuring 150 mm × 15 mm. The initial clamping distance and the velocity were set at 100 mm and 100 mm/min, respectively.

2.4.6. Water contact angle (WCA)

A contact angle goniometer (JC2000C1, Shanghai Chen Digital Technology Instrument Co., Ltd., China) was utilized to measure the spread of water droplets on the film surface using the sessile droplet method. The contour data of water droplets were fit using the Laplace-Young equation (Zhang et al., 2023c).

2.4.7. Water vapor permeability (WVP)

The WVP of the films was determined using a WVP tester (W3/031, Labthink Instruments Co., Ltd., Jinan, China). Round films with a diameter of 80 mm were tested at 38.0°C and 90% relative humidity (RH) with a preheating time of 4 h and a weighing interval of 2 h. The WVP value was calculated from triplicate measurements.

2.4.8. Water solubility (WS)

WS was determined according to the method of Gao et al. (2022) with some modifications. The films were cut into samples measuring 40 mm × 40 mm and dried at 40°C until a constant weight (m_1) was achieved over 24 h. Subsequently, the dried film samples were immersed in 50 mL of distilled water for 24 h, then removed, dried again at 60°C for 24 h, and weighed (m_2). The calculation method for WS (%) was as follows:

$$WS = \frac{m_1 - m_2}{m_2}$$

2.4.9. Thermogravimetric (TG) analysis

Thermal degradation behavior was measured using a TG analyzer (TGDTA7300, Hitachi, Ltd., Japan). The TG test involved placing 10 mg of film sample in an alumina crucible and heating it in the range of 40-600°C with a heating rate of 10°C/min and an N_2 flow rate of 50 mL/min. Derivative TG (DTG) curves were derived from the differential of TG values.

2.4.10. Release of essential oils in different food simulants

Two food simulants were selected: 10% ethanol (for aqueous-based foods) and 90%

ethanol (for fatty foods). Film samples measuring 20 × 40 mm were immersed in 10 mL of food simulants, and 2 mL of the solutions were removed at specific time intervals at room temperature to determine the released GEO. Subsequently, 2 mL of the simulant solutions were added to maintain the original conditions. The release of GEO from the films was measured using a UV-visible spectrophotometer at 278 nm (Zhang et al., 2021).

2.4.11. Antioxidant properties

The DPPH and ABTS radical scavenging rate (%) of the films were determined using a previous method with some modifications (Shen et al., 2021).

A 50 mg film was immersed in 10 mL of anhydrous ethanol and shaken for 4 h at 25°C. Subsequently, 1 mL of the film extract solution was mixed with 3 mL of 0.1 mM DPPH anhydrous ethanol solution and reacted in the dark for 30 min. Afterward, the absorbance at 517 nm was measured.

Equal amounts of ABTS (7 mM) solution and $K_2S_2O_8$ solution (2.45 mM) were mixed and placed in the dark for 12 h. The absorbance of the mixed solution was then adjusted to be 0.70 ± 0.02 (at 734 nm) to prepare the ABTS working solution. Subsequently, 200 μL of film extract solution was mixed with 3 mL of ABTS working solution and reacted in the dark for 30 min. Afterward, the absorbance at 734 nm was measured. The DPPH radical scavenging activity (%) and ABTS radical scavenging activity (%) were calculated as follows:

$$scavenging\ rate(\%) = 1 - \frac{A_1 - A_2}{A_O} \times 100$$

where A_1 is the absorbance of the sample, A_0 is the absorbance measured under the same conditions with anhydrous ethanol instead of the film extract solution, and A_2 is the absorbance measured with anhydrous ethanol instead of DPPH or ABTS.

2.4.12. Antibacterial properties

The antibacterial activity of the films against *S. aureus* and *E. coli* was analyzed using

the disc diffusion method (Hasheminya et al., 2019). Pathogens were inoculated and streaked on Mueller-Hinton agar medium, which was then incubated at 37°C for 12 h. The bacterial cultures were subsequently transferred to 0.85% (w/v) NaCl solution to adjust the turbidity of the bacterial suspension to 0.5 McFarland (1.5 × 10^8 CFU/mL). The bacterial suspension was then evenly spread onto Mueller-Hinton agar plates using a cotton swab. Sterile filter paper discs (6 mm) were immersed in the film extraction solution and placed on the agar surface using forceps. The plates were then incubated at 37°C for 24 h. After incubation, the antibacterial activity was assessed by measuring the size of the zone of inhibition surrounding the discs.

2.5. Statistical analysis

SPSS statistical software version 22.0 (SPSS Inc., Chicago, USA) was applied to analyze the Data, and the difference between the mean values was analyzed by Waller-Duncan's multiple range test at the significance level of $p < 0.05$.

3. Results and discussion

3.1 Characterization of GEO-NEs

Oil-in-water (O/W) type GEO-NEs were prepared using the ultrasonic emulsification method. As depicted in Fig. 2A, the average particle size of the GEO-NEs was 176.4±1.2 nm, with a PDI of 0.276±0.012, indicating the homogeneous dispersion of the GEO-NEs droplets. This observation was further confirmed by microscopy images (Fig. 2B). GEO-NEs were formulated using Tween 80, a non-ionic surfactant, with steric repulsion as the primary mechanism for stabilizing the nanoemulsion (Campolo et al., 2020). Consequently, the zeta potential of the nanoemulsion is expected to approximate zero, whereas nanoemulsions stabilized by electrostatic repulsion require a zeta potential of at least ±30 mV (Zhang et al., 2022). The zeta potential of GEO-NEs was measured to be -12.37±0.05 mV, indicating a negative surface charge, which may be attributed to the dissociation of ionizable compounds present in GEO (Campolo et al., 2020; Hasheminya & Dehghannya, 2021). Additionally, no phase separation was observed for GEO-NEs after storage at 4°C and 25°C for 28 days (Fig. 2C), and there

were no significant changes in the average particle size and PDI (Fig. 2D), indicating the excellent stability of GEO-NEs.

3.2. Characterizations of composite films

3.2.1 Fourier transform infrared (FT-IR) analysis

The intermolecular interactions within the film matrix were analyzed using FTIR spectroscopy. As illustrated in Fig. 3A, a broad and strong band was observed in the range of 3500-3300 cm^{-1}, attributed to the stretching vibrations of hydroxyl groups (-OH) present in PVA, xylan, and glycerol (Wang et al., 2022; Yang et al., 2024). A gradual shift of the peak from 3290 cm^{-1} to 3280 cm^{-1} was noted in the wavenumber of films containing GEO-NEs compared to the control group, implying the formation of hydrogen bonds between GEO-NEs and the film matrix (Wu et al., 2023). Their potential hydrogen-bonding interactions are depicted in Fig. 3C. The weak band around 2927 cm^{-1} was related to the stretching vibrations of C-H in the CH_2 and CH_3 groups. Additionally, films containing GEO-NEs all exhibited a characteristic peak at 1740 cm^{-1}, with the peak amplitude progressively strengthening with increasing concentrations of GEO-NEs. This peak was associated with the C=O stretching vibration of the aldehyde or ester carbonyl groups of GEO. Similar findings were reported by Cai and Wang (2021). The characteristic peaks at 1417 and 1034 cm^{-1} corresponded to the stretching vibrations of -C-H and C-O-C in the pyranose ring of xylan, respectively, and the β-pyranose configuration of xylan was confirmed by the characteristic peak at 846 cm^{-1} (Liu et al., 2019b; Shahrampour & Razavi, 2023). FTIR results indicated that hydrogen bonding dominated the interaction between the GEOs-NEs and the xylan/PVA base matrix, and GEOs-NEs did not change the chemical structure of the films.

3.2.2 X-ray diffraction (XRD) analysis

The crystal structure of the films was investigated using XRD. As depicted in Fig. 3B, a prominent diffraction peak was observed at $2\theta = 19.3°$ for all films. Importantly, the incorporation of GEO-NEs did not result in any new diffraction peaks, suggesting that

GEO-NEs did not induce alterations in the crystal structure of the xylan/PVA base matrix. This observation validates the compatibility between GEO-NEs and the film matrix (Fan et al., 2023). However, the incorporation of GEO-NEs resulted in a reduction in the crystallinity of the films. This effect was particularly noticeable at GEO-NEs concentrations of 2% and 4%, where a weakening in the intensity of the film diffraction peaks was observed. On the one hand, FTIR analysis confirmed the formation of new hydrogen bonds among GEO-NEs and the film matrix, thereby weakening the original ordered structure formed by xylan and PVA, consequently reducing the crystallinity (Liu et al., 2019b). On the other hand, reduced crystallinity implies increased mobility among xylan and PVA molecules, which may affect the mechanical properties of the films, such as elongation at break (Tavassoli et al., 2021).

3.2.3 SEM analysis

The surface and cross-section SEM micrographs of films are presented in Fig. 4. The control film appeared smooth and continuous without any pores, confirming the good compatibility between xylan and PVA. However, as the concentration of GEO-NEs increased, the film surfaces became rougher, and pores began to appear in the cross-sections. This phenomenon was particularly noticeable at GEO-NEs concentrations of 6% and 8%. The presence of pores and roughness can be attributed to the high concentration of GEO-NEs hindering the ability of the film matrix to capture more oil droplets through hydrogen bonding. This leads to increased flocculation and coalescence of oil droplets during the film formation process, causing them to migrate towards the film surface and resulting in a non-homogeneous morphology. Additionally, the evaporation of the oil droplets during this process contributes to the formation of pores (Acevedo-Fani, Salvia-Trujillo, Rojas-Graü, & Martín-Belloso, 2015; Hasheminya et al., 2021; Zhang et al., 2021). Similar observations have been reported in other studies where biopolymer-based films became rough and porous after mixing with EO-NEs (Cai et al., 2021; Chu et al., 2020; Fan et al., 2024; Norcino et al., 2020). These changes in microstructure may affect the barrier properties of the film, such as water barrier performance (Hasheminya et al., 2021), as confirmed in section 3.2.7.

3.2.4 Optical properties

As shown in Table S1, with the increasing concentration of GEO-NEs, the L* and a* values of the composite film decreased while b* increased, indicating that the film became darker and more yellowish. Moreover, the opacity gradually increased, which is attributed to light scattering caused by the surface roughness and internal porous structures of the film (Lin et al., 2020). Transparency is particularly important for food packaging materials, as foods retaining their original colors and appearances are more likely to be accepted by consumers (Liu et al., 2022). From a visual perspective (Fig. 5A), the composite film containing 8% GEO-NEs still exhibited relatively high transparency.

The UV transmittance of the films is illustrated in Fig. 5B. It can be observed that the incorporation of GEO-NEs effectively shielded the spectra of UVC (275-200 nm), UVB (320-275 nm), and UVA (400-320 nm), which significantly enhanced the UV shielding performance of the films. The light scattering by the small lipid droplets of the nanoemulsion and the absorption of UV and visible light by the phenolic compounds in the GEO may be responsible for the enhanced UV shielding performance of the films (Chen et al., 2016; Fu et al., 2023), which is positive for inhibiting the oxidative deterioration of foodstuffs (Zhang et al., 2023c).

3.2.5 Mechanical properties

Mechanical properties are crucial attributes of films, ensuring their ability to withstand external stresses during transportation, handling, and storage. Tensile strength (TS) and elongation at break (EAB) represent the strength and flexibility of the films, respectively (Erfanifar, Majdinasab, & Shaghaghian, 2023). As illustrated in Fig. 5C and D, the xylan/PVA composite films exhibited the capability to withstand various deformations, with their TS and EAB comparable to the mechanical properties of the prevalent commercial packaging material, high-density polyethylene (HDPE) (TS, approximately 22-23 MPa; EAB, approximately 150%) (Lee, Garcia, Shin, & Kim, 2019). As the concentration of GEO-NEs increased, the TS gradually decreased from

27.38±3.25 MPa in the control film to 20.27±2.55 MPa in the 8% GEO-NEs film. Conversely, the EAB of the films significantly increased ($p<0.05$) and reached its maximum at a moderate concentration (GEO-NEs 4%), measuring 258.4±38.6%. Due to the weakened hydrogen bonding between xylan and PVA caused by GEO-NEs, the cohesive forces of the film matrix were reduced, resulting in a lower TS (Almasi, Azizi, & Amjadi, 2020; Zhang et al., 2021). At the same time, the chain entanglement of xylan and PVA was weakened, leading to an increase in molecular mobility and consequently enhancing the EAB (Chen et al., 2016). These results were also verified in the XRD analysis. It is worth noting that the continued addition of GEO-NEs resulted in a reduction in EAB. This may be attributed to the uneven dispersion of high concentrations of GEO-NEs within the film matrix, leading to flocculation and the formation of localized hardened regions during the film formation process. Ultimately, this phenomenon affected the overall flexibility of the thin film.

3.2.6 Thermostability

The thermostability of the films was investigated using thermogravimetric analysis (TGA) and the first derivative of TGA curves (DTG). As shown in Fig. 5E, the films exhibited multiple stages of weight loss within the temperature range of 40-600°C. The initial stage of weight loss (40-120°C) was attributed to the loss of moisture from the film matrix. Subsequently, a second stage of weight loss occurred in the temperature range of 150-250°C, attributed to the degradation of glycerol and PVA chains (Chen, Ren, & Meng, 2015). A third stage of weight loss was observed between 250-330°C, involving further degradation of PVA chains and degradation of xylan chains (Liu et al., 2019b; Wang et al., 2014). In the final stage, from 350-600°C, polymer matrix carbonization occurred, leading to a stabilization of film mass loss (Zhang et al., 2023b). In Fig. 5F, it was observed that the maximum thermal degradation rate of the film was achieved at around 320°C. The maximum thermal degradation temperature (T_{max}) reflects the thermostability of the film, with a higher T_{max} indicating better thermal stability (Qin et al., 2022). Compared to the control group with a T_{max} of 322.9°C, the T_{max} for films containing 2%, 4%, 6%, and 8% of GEO-NEs were 326.6°C, 322.3°C,

325.4°C, and 325.9°C, respectively, showing a slight improvement in thermostability. In summary, the inclusion of GEO-NEs exerted negligible influence on the thermostability of the xylan/PVA films.

3.2.7 WCA, WS and WVP analysis

Film surface hydrophobicity was assessed by WCA, with $\theta > 65°$ generally indicating a hydrophobic surface (Zhang et al., 2023c). As shown in Fig. 6A, all films exhibited hydrophilic surfaces, which can be attributed to the inherent hydrophilic properties of xylan and PVA in the film-forming matrix. The control film had the highest WCA of 50.1 ± 3.9°. However, with the increasing concentration of GEO-NEs, there was a significant decrease in the WCA of films ($P < 0.05$). This decrease can be associated with the strong surface hydrophilicity of GEO-NEs droplets, as Tween80 and GEO can form emulsion droplets with hydrophilic tails pointing to the aqueous solution (Liu et al., 2022). WCA was also influenced by the surface roughness and porosity of the film (Liu et al., 2019a; Qin et al., 2022). Higher surface roughness and internal porous structures increased the surface area of the film in contact with water molecules, leading to increased hydrophilicity or even water solubility of the film (Fig. 6B).

The efficiency of moisture penetration through the film was assessed by determining the WVP. A higher WVP indicates insufficient water barrier properties of the film, which would create favorable conditions for microbial growth and lead to food spoilage. As illustrated in Fig. 6C, there was a significant decrease followed by a remarkably increased trend in WVP with increasing concentration of GEO-NEs ($P < 0.05$). Compared to the WVP of the control film, which was $10.45 \pm 0.72\times10^{-13}$ $g\cdot cm^{-1}\cdot s^{-1}\cdot Pa^{-1}$, the film containing 2% GEO-NEs exhibited the lowest WVP of $7.45 \pm 0.71\times10^{-13}$ $g\cdot cm^{-1}\cdot s^{-1}\cdot Pa^{-1}$. The decrease in WVP is associated with an increase in the tortuosity of the path of water molecules through the film. On the one hand, GEO-NEs droplets at low concentrations were able to disperse uniformly in the film matrix, thereby increasing the length of the path for water molecules through the film (Hasheminya et al., 2021). On the other hand, XRD results indicated that GEO-NEs caused discontinuities in the film matrix, which could potentially further increase the tortuosity

path. However, films containing high concentrations of GEO-NEs (6% and 8%) exhibited a large number of pores within their structure, which provided additional space and channels for water molecules to traverse through the film, thus causing an increase in WVP (Mirsharifi et al., 2023; Rui et al., 2024). Despite the significant improvement in water barrier performance observed in composite films containing 2% GEO-NEs, their WVP remains higher than that of commercial low-density polyethylene (LDPE) films, which typically exhibit a WVP of approximately 7.00×10^{-14} $g\cdot m^{-1}\cdot s^{-1}\cdot Pa^{-1}$ (Silva et al., 2024). Therefore, further research is required to improve the water barrier performance, it is also the direction of future efforts for bio-based packaging materials.

3.2.8 Release of GEO in different food simulants

The release curves of GEO in two different food simulants are shown in Fig. 7. Initially, GEO exhibited a rapid release, which gradually decelerated until reaching a constant level. As described by Dong et al. (2024), water molecules initially diffused from the simulated solution into the film matrix, resulting in swelling and dissolution of the film, which led to the detachment of GEO from the film matrix and its subsequent release into the simulated solution until achieving thermodynamic equilibrium. Due to the higher hydrophilicity of the xylan/PVA composite film, its swelling phenomenon was more obvious in a 10% ethanol solution with lower polarity, which led to a faster release of GEO and reached equilibrium in a shorter time. Fig. 7 also demonstrates that the release rate of GEO in both simulated systems decreased with increasing concentration of GEO-NEs. This trend can be explained by the reduction in the mass transfer concentration gradient, as the increasing accumulation of GEO in the simulant reduced the concentration gradient between the film matrix and the simulant, making the release of GEO to the simulant slower (Xu et al., 2019).

3.2.9 Antioxidant and antimicrobial activities

As shown in Fig. 8A, xylan/PVA films without GEO-NEs also exhibited certain antioxidant activity, with DPPH and ABTS radical scavenging rates of 5.53±1.20% and

11.06±1.22%, respectively, which was related to the fact that xylan (derived from corn cobs) as a reducing polysaccharide branched by arabinose and glucuronic acid (Bao et al., 2018). With the increase in GEO-NEs concentration, the antioxidant activity of the composite films significantly increased ($P < 0.05$). Films containing 8% GEO-NEs showed a 45.90% and 59.87% increase in DPPH and ABTS radical scavenging rates, respectively, compared to the control films. A study by Badrunanto et al. (2024), indicated that terpene compounds such as β-myrcene, D-limonene, α-sabinene, geranyl acetate, α-curcumene, α-zingiberene, α-farnesene, β-bisabolene, and β-sesquiphellandrene were closely associated with the antioxidant activity of GEO.

The antimicrobial activity of the films was assessed using the disc diffusion method, as depicted in Fig. 8B. It was noted that inhibition zones against both Gram-positive bacteria (*S. aureus*) and Gram-negative bacteria (*E. coli*) were observed when the concentration of GEO-NEs in the film reached 6%. Similar findings were reported by Zhang et al. (2021) and Mutlu (2023), suggesting that the films exhibited antimicrobial activity only upon the addition of high concentrations of EO-NEs. Generally, Gram-negative bacteria tend to exhibit greater tolerance to EOs when compared to Gram-positive bacteria. Apart from the peptidoglycan layer, the outer membrane of Gram-negative bacteria contains lipopolysaccharides, rendering the diffusion of hydrophobic EOs into the cells more challenging (Zhang et al., 2023a). However, in this study, it was observed that composite films strongly inhibited *E. coli* compared to *S. aureus*. This could be attributed to the accumulation of certain specific hydrophobic compounds from the essential oils on the outer membrane of *E. coli*, disrupting its permeability and inhibiting bacterial growth (Ran et al., 2023). Additionally, studies have also reported controversies regarding the effectiveness of black pepper essential oil (Acharya et al., 2024; Amalraj, Haponiuk, Thomas, & Gopi, 2020; Saranti et al., 2021), oregano essential oil (Hosseini, Rezaei, Zandi, & Farahmandghavi, 2015; Lee et al., 2019), and cinnamon essential oil (Ran et al., 2023; Wu et al., 2023) in various film matrixes against both Gram-positive and Gram-negative bacteria. In conclusion, numerous factors, including the type of film matrix, the type and concentration of EOs, as well as the initial number of bacteria and growth conditions, collectively influenced the

antibacterial activity of the films (Hasheminya et al., 2021).

4. Conclusion

In this study, active films with UV resistance, antioxidant, and antimicrobial properties were prepared using xylan and PVA as the film-forming matrix and blended with GEO-NEs. The results indicated good compatibility among xylan, PVA, and GEO-NEs. The incorporation of GEO-NEs improved the UV shielding properties, with films containing 8% GEO-NEs maintaining high transparency. Despite a decrease in tensile strength and an increase in elongation at break, the mechanical properties of all films met the standards of commercial packaging material HDPE. Furthermore, the antioxidant activities of xylan/PVA films were significantly enhanced upon the addition of GEO-NEs, exhibiting inhibitory activities against both *S. aureus* and *E. coli* at a 6% concentration. Therefore, xylan/PVA films containing GEO-NEs demonstrate potential applications as active packaging materials. However, further research is needed to improve their hydrophobicity and water barrier properties.

Declaration of competing interest

The authors declare no conflict of interest.

Acknowledgements

This research was supported by the *Key R&D* Project of Shandong Province (2023TZXD070).

References

Acevedo-Fani, A., Salvia-Trujillo, L., Rojas-Graü, M. A., & Martín-Belloso, O. (2015). Edible films from essential-oil-loaded nanoemulsions: Physicochemical characterization and antimicrobial properties. *Food Hydrocolloids, 47*, 168-177. https://doi.org/https://doi.org/10.1016/j.foodhyd.2015.01.032

Acharya, D. R., Liu, S., Lu, H., Albashir, D., Koirala, P., Shi, Y., & Chen, Q. (2024). Nanoemulsion-integrated gelatin/bacterial cellulose nanofibril-based multifunctional film: Fabrication, characterization, and application. *International Journal of Biological Macromolecules, 257*, 128341. https://doi.org/https://doi.org/10.1016/j.ijbiomac.2023.128341

Almasi, H., Azizi, S., & Amjadi, S. (2020). Development and characterization of pectin films activated by nanoemulsion and Pickering emulsion stabilized marjoram (*Origanum majorana* L.) essential oil. *Food Hydrocolloids, 99*, 105338. https://doi.org/https://doi.org/10.1016/j.foodhyd.2019.105338

Amalraj, A., Haponiuk, J. T., Thomas, S., & Gopi, S. (2020). Preparation, characterization and antimicrobial activity of polyvinyl alcohol/gum arabic/chitosan composite films incorporated with black pepper essential oil and ginger essential oil. *International Journal of Biological Macromolecules, 151*, 366-375. https://doi.org/https://doi.org/10.1016/j.ijbiomac.2020.02.176

Badrunanto, Wahyuni, W. T., Farid, M., Batubara, I., & Yamauchi, K. (2024). Antioxidant components of the three different varieties of Indonesian ginger essential oil: In vitro and computational studies. *Food Chemistry Advances, 4*, 100558. https://doi.org/https://doi.org/10.1016/j.focha.2023.100558

Bao, Y., Zhang, H., Luan, Q., Zheng, M., Tang, H., & Huang, F. (2018). Fabrication of cellulose nanowhiskers reinforced chitosan-xylan nanocomposite films with antibacterial and antioxidant activities. *Carbohydrate Polymers, 184*, 66-73. https://doi.org/https://doi.org/10.1016/j.carbpol.2017.12.051

Cai, L., & Wang, Y. (2021). Physicochemical and antioxidant properties based on fish sarcoplasmic protein/chitosan composite films containing ginger essential oil nanoemulsion. *Food and Bioprocess Technology, 14*(1), 151-163. https://doi.org/10.1007/s11947-020-02564-0

Campolo, O., Giunti, G., Laigle, M., Michel, T., & Palmeri, V. (2020). Essential oil-based nano-emulsions: Effect of different surfactants, sonication and plant species on physicochemical characteristics. *Industrial Crops and Products, 157*, 112935. https://doi.org/https://doi.org/10.1016/j.indcrop.2020.112935

Chen, H., Hu, X., Chen, E., Wu, S., McClements, D. J., Liu, S., . . . Li, Y. (2016). Preparation, characterization, and properties of chitosan films with cinnamaldehyde nanoemulsions. *Food Hydrocolloids, 61*, 662-671. https://doi.org/https://doi.org/10.1016/j.foodhyd.2016.06.034

Chen, K., Tian, R., Jiang, J., Xiao, M., Wu, K., Kuang, Y., . . . Jiang, F. (2024). Moisture loss inhibition with biopolymer films for preservation of fruits and vegetables: A review. *International Journal of Biological Macromolecules, 263*, 130337. https://doi.org/https://doi.org/10.1016/j.ijbiomac.2024.130337

Chen, X., Ren, J., & Meng, L. (2015). Influence of ammonium zirconium carbonate on

properties of poly(vinyl alcohol)/xylan composite films. *Journal of Nanomaterials, 2015*, 810464. https://doi.org/10.1155/2015/810464

Chu, Y., Cheng, W., Feng, X., Gao, C., Wu, D., Meng, L., . . . Tang, X. (2020). Fabrication, structure and properties of pullulan-based active films incorporated with ultrasound-assisted cinnamon essential oil nanoemulsions. *Food Packaging and Shelf Life, 25*, 100547. https://doi.org/https://doi.org/10.1016/j.fpsl.2020.100547

Curry, T. M., Peña, M. J., & Urbanowicz, B. R. (2023). An update on xylan structure, biosynthesis, and potential commercial applications. *Cell Surface, 9*, 100101. https://doi.org/https://doi.org/10.1016/j.tcsw.2023.100101

Dong, J., Yu, D., Zhang, L., Wang, G., Zhang, P., You, Y., . . . Xia, W. (2024). Chitosan/alginate dialdehyde trilayer films with cinnamaldehyde nanoemulsions for grass carp preservation. *Food Hydrocolloids, 147*, 109413. https://doi.org/https://doi.org/10.1016/j.foodhyd.2023.109413

Erfanifar, Z., Majdinasab, M., & Shaghaghian, S. (2023). Production and characterization of sage seed gum bioactive film containing Zataria multiflora essential oil nanoemulsion. *Food Chemistry, 408*, 134871. https://doi.org/https://doi.org/10.1016/j.foodchem.2022.134871

Fan, S., Wang, D., Wen, X., Li, X., Fang, F., Richel, A., . . . Zhang, D. (2023). Incorporation of cinnamon essential oil-loaded Pickering emulsion for improving antimicrobial properties and control release of chitosan/gelatin films. *Food Hydrocolloids, 138*, 108438. https://doi.org/https://doi.org/10.1016/j.foodhyd.2022.108438

Fan, S., Yin, X., Liu, X., Wang, G., & Qiu, W. (2024). Enhancing bread preservation through non-contact application of starch-based composite film infused with clove essential oil nanoemulsion. *International Journal of Biological Macromolecules, 263*, 130297. https://doi.org/https://doi.org/10.1016/j.ijbiomac.2024.130297

Fu, H., Huang, R., Li, J., Lin, Z., Wei, F., & Lin, B. (2023). Multifunctional cinnamaldehyde-tannic acid nano-emulsion/chitosan composite film for mushroom preservation. *Food Hydrocolloids, 145*, 109111. https://doi.org/https://doi.org/10.1016/j.foodhyd.2023.109111

Gao, S., Zhang, Y., Wang, J., Jiang, J., Zhai, X., Wang, W., & Hou, H. (2022). Influence of starch content on the physicochemical and antimicrobial properties of starch/PBAT/ε-polylysine hydrochloride blown films. *Food Packaging and Shelf Life, 34*, 101005. https://doi.org/https://doi.org/10.1016/j.fpsl.2022.101005

Hasheminya, S.-M., & Dehghannya, J. (2021). Development and characterization of novel edible films based on *Cordia dichotoma* gum incorporated with *Salvia mirzayanii* essential oil nanoemulsion. *Carbohydrate Polymers, 257*, 117606. https://doi.org/https://doi.org/10.1016/j.carbpol.2020.117606

Hasheminya, S.-M., Mokarram, R. R., Ghanbarzadeh, B., Hamishekar, H., Kafil, H. S., & Dehghannya, J. (2019). Influence of simultaneous application of copper oxide nanoparticles and *Satureja Khuzestanica* essential oil on properties of

kefiran–carboxymethyl cellulose films. *Polymer Testing, 73*, 377-388. https://doi.org/https://doi.org/10.1016/j.polymertesting.2018.12.002

He, J., Hadidi, M., Yang, S., Khan, M. R., Zhang, W., & Cong, X. (2023). Natural food preservation with ginger essential oil: Biological properties and delivery systems. *Food Research International, 173*, 113221. https://doi.org/https://doi.org/10.1016/j.foodres.2023.113221

Höije, A., Gröndahl, M., Tømmeraas, K., & Gatenholm, P. (2005). Isolation and characterization of physicochemical and material properties of arabinoxylans from barley husks. *Carbohydrate Polymers, 61*(3), 266-275. https://doi.org/https://doi.org/10.1016/j.carbpol.2005.02.009

Hosseini, S. F., Rezaei, M., Zandi, M., & Farahmandghavi, F. (2015). Bio-based composite edible films containing Origanum vulgare L. essential oil. *Industrial Crops and Products, 67*, 403-413. https://doi.org/https://doi.org/10.1016/j.indcrop.2015.01.062

Jurić, M., Maslov Bandić, L., Carullo, D., & Jurić, S. (2024). Technological advancements in edible coatings: Emerging trends and applications in sustainable food preservation. *Food Bioscience, 58*, 103835. https://doi.org/https://doi.org/10.1016/j.fbio.2024.103835

Kong, R., Wang, J., Cheng, M., Lu, W., Chen, M., Zhang, R., & Wang, X. (2020). Development and characterization of corn starch/PVA active films incorporated with carvacrol nanoemulsions. *International Journal of Biological Macromolecules, 164*, 1631-1639. https://doi.org/https://doi.org/10.1016/j.ijbiomac.2020.08.016

Lakshmayya, N. S. V., Mishra, A. K., Mohanta, Y. K., Panda, J., Naik, B., Mishra, B., & Varma, R. S. (2023). Essential oils-based nano-emulsion system for food safety and preservation: Current status and future prospects. *Biocatalysis and Agricultural Biotechnology, 53*, 102897. https://doi.org/https://doi.org/10.1016/j.bcab.2023.102897

Lee, J. Y., Garcia, C. V., Shin, G. H., & Kim, J. T. (2019). Antibacterial and antioxidant properties of hydroxypropyl methylcellulose-based active composite films incorporating oregano essential oil nanoemulsions. *LWT, 106*, 164-171. https://doi.org/https://doi.org/10.1016/j.lwt.2019.02.061

Li, Q., Chen, Z., Zeng, L., Bi, Y., Kong, F., Wang, Z., & Tan, S. (2023). Characterization, in-vitro digestion, antioxidant, anti-hyperlipidemic and antibacterial activities of *Zanthoxylum bungeanum* Maxim essential oil nano-emulsion. *Food Bioscience, 56*, 103082. https://doi.org/https://doi.org/10.1016/j.fbio.2023.103082

Li, X., Yang, X., Deng, H., Guo, Y., & Xue, J. (2020). Gelatin films incorporated with thymol nanoemulsions: Physical properties and antimicrobial activities. *International Journal of Biological Macromolecules, 150*, 161-168. https://doi.org/https://doi.org/10.1016/j.ijbiomac.2020.02.066

Li, Z., Jiang, X., Huang, H., Liu, A., Liu, H., Abid, N., & Ming, L. (2022). Chitosan/zein films incorporated with essential oil nanoparticles and nanoemulsions: Similarities and differences. *International Journal of Biological*

Macromolecules, 208, 983-994. https://doi.org/https://doi.org/10.1016/j.ijbiomac.2022.03.200

Lin, D., Zheng, Y., Wang, X., Huang, Y., Ni, L., Chen, X., . . . Wu, D. (2020). Study on physicochemical properties, antioxidant and antimicrobial activity of okara soluble dietary fiber/sodium carboxymethyl cellulose/thyme essential oil active edible composite films incorporated with pectin. *International Journal of Biological Macromolecules, 165*, 1241-1249. https://doi.org/https://doi.org/10.1016/j.ijbiomac.2020.10.005

Liu, J., Liu, Y., Shao, S., Zheng, X., & Tang, K. (2022). Soluble soybean polysaccharide/carboxymethyl chitosan coatings incorporated with lavender essential oil: Structure, properties and application in fruit preservation. *Progress in Organic Coatings, 173*, 107178. https://doi.org/https://doi.org/10.1016/j.porgcoat.2022.107178

Liu, Q., Wang, W., Qi, J., Huang, Q., & Xiao, J. (2019a). Oregano essential oil loaded soybean polysaccharide films: Effect of Pickering type immobilization on physical and antimicrobial properties. *Food Hydrocolloids, 87*, 165-172. https://doi.org/https://doi.org/10.1016/j.foodhyd.2018.08.011

Liu, X., Chen, X., Ren, J., Chang, M., He, B., & Zhang, C. (2019b). Effects of nano-ZnO and nano-SiO_2 particles on properties of PVA/xylan composite films. *International Journal of Biological Macromolecules, 132*, 978-986. https://doi.org/https://doi.org/10.1016/j.ijbiomac.2019.03.088

Mikkonen, K. S., Laine, C., Kontro, I., Talja, R. A., Serimaa, R., & Tenkanen, M. (2015). Combination of internal and external plasticization of hydroxypropylated birch xylan tailors the properties of sustainable barrier films. *European Polymer Journal, 66*, 307-318. https://doi.org/https://doi.org/10.1016/j.eurpolymj.2015.02.034

Mirsharifi, S. M., Sami, M., Jazaeri, M., & Rezaei, A. (2023). Production, characterization, and antimicrobial activity of almond gum/polyvinyl alcohol/chitosan composite films containing thyme essential oil nanoemulsion for extending the shelf-life of chicken breast fillets. *International Journal of Biological Macromolecules, 227*, 405-415. https://doi.org/https://doi.org/10.1016/j.ijbiomac.2022.12.183

Mutlu, N. (2023). Effects of grape seed oil nanoemulsion on physicochemical and antibacterial properties of gelatin-sodium alginate film blends. *International Journal of Biological Macromolecules, 237*, 124207. https://doi.org/https://doi.org/10.1016/j.ijbiomac.2023.124207

Norcino, L. B., Mendes, J. F., Natarelli, C. V. L., Manrich, A., Oliveira, J. E., & Mattoso, L. H. C. (2020). Pectin films loaded with copaiba oil nanoemulsions for potential use as bio-based active packaging. *Food Hydrocolloids, 106*, 105862. https://doi.org/https://doi.org/10.1016/j.foodhyd.2020.105862

Oun, A. A., Shin, G. H., Rhim, J.-W., & Kim, J. T. (2022). Recent advances in polyvinyl alcohol-based composite films and their applications in food packaging. *Food Packaging and Shelf Life, 34*, 100991. https://doi.org/https://doi.org/10.1016/j.fpsl.2022.100991

Pandey, V. K., Islam, R. U., Shams, R., & Dar, A. H. (2022). A comprehensive review on the application of essential oils as bioactive compounds in Nano-emulsion based edible coatings of fruits and vegetables. *Applied Food Research, 2*(1), 100042. https://doi.org/https://doi.org/10.1016/j.afres.2022.100042

Qin, C., Yang, G., Zhu, C., & Wei, M. (2022). Characterization of edible film fabricated with HG-type hawthorn pectin gained using different extraction methods. *Carbohydrate Polymers, 285*, 119270. https://doi.org/https://doi.org/10.1016/j.carbpol.2022.119270

Ran, R., Zheng, T., Tang, P., Xiong, Y., Yang, C., Gu, M., & Li, G. (2023). Antioxidant and antimicrobial collagen films incorporating Pickering emulsions of cinnamon essential oil for pork preservation. *Food Chemistry, 420*, 136108. https://doi.org/https://doi.org/10.1016/j.foodchem.2023.136108

Rao, J., Lv, Z., Chen, G., Hao, X., Guan, Y., & Peng, F. (2021). Fabrication of flexible composite film based on xylan from pulping process for packaging application. *International Journal of Biological Macromolecules, 173*, 285-292. https://doi.org/https://doi.org/10.1016/j.ijbiomac.2021.01.128

Rui, L., Li, Y., Wu, X., Wang, Y., & Xia, X. (2024). Effect of clove essential oil nanoemulsion on physicochemical and antioxidant properties of chitosan film. *International Journal of Biological Macromolecules, 263*, 130286. https://doi.org/https://doi.org/10.1016/j.ijbiomac.2024.130286

Sanchez, L. T., Pinzon, M. I., & Villa, C. C. (2022). Development of active edible films made from banana starch and curcumin-loaded nanoemulsions. *Food Chemistry, 371*, 131121. https://doi.org/https://doi.org/10.1016/j.foodchem.2021.131121

Saranti, T. F. d. S., Melo, P. T. S., Cerqueira, M. A., Aouada, F. A., & de Moura, M. R. (2021). Performance of gelatin films reinforced with cloisite Na^{+} and black pepper essential oil loaded nanoemulsion. *Polymers, 13*(24). https://doi.org/10.3390/polym13244298

Sárossy, Z., Tenkanen, M., Pitkänen, L., Bjerre, A.-B., & Plackett, D. (2013). Extraction and chemical characterization of rye arabinoxylan and the effect of β-glucan on the mechanical and barrier properties of cast arabinoxylan films. *Food Hydrocolloids, 30*(1), 206-216. https://doi.org/https://doi.org/10.1016/j.foodhyd.2012.05.022

Shahrampour, D., & Razavi, S. M. A. (2023). Fabrication and characterization of novel biodegradable active films based on Eremurus luteus root gum incorporated with nanoemulsions of rosemary essential oil. *Progress in Organic Coatings, 175*, 107360. https://doi.org/https://doi.org/10.1016/j.porgcoat.2022.107360

Shen, Y., Ni, Z.-J., Thakur, K., Zhang, J.-G., Hu, F., & Wei, Z.-J. (2021). Preparation and characterization of clove essential oil loaded nanoemulsion and pickering emulsion activated pullulan-gelatin based edible film. *International Journal of Biological Macromolecules, 181*, 528-539. https://doi.org/https://doi.org/10.1016/j.ijbiomac.2021.03.133

Shi, Y., Zhang, M., Chen, K., & Wang, M. (2022). Nano-emulsion prepared by high pressure homogenization method as a good carrier for Sichuan pepper essential oil: Preparation, stability, and bioactivity. *LWT, 154*, 112779.

https://doi.org/https://doi.org/10.1016/j.lwt.2021.112779
Silva, J. M., Vilela, C., Girão, A. V., Branco, P. C., Martins, J., Freire, M. G., . . . Freire, C. S. R. (2024). Wood inspired biobased nanocomposite films composed of xylans, lignosulfonates and cellulose nanofibers for active food packaging. Carbohydrate Polymers, 337, 122112. https://doi.org/https://doi.org/10.1016/j.carbpol.2024.122112.
Šimkovic, I., Kelnar, I., Uhliariková, I., Mendichi, R., Mandalika, A., & Elder, T. (2014). Carboxymethylated-, hydroxypropylsulfonated- and quaternized xylan derivative films. *Carbohydrate Polymers, 110*, 464-471. https://doi.org/https://doi.org/10.1016/j.carbpol.2014.04.055
Singh, I. R., & Pulikkal, A. K. (2022). Preparation, stability and biological activity of essential oil-based nano emulsions: A comprehensive review. *OpenNano, 8*, 100066. https://doi.org/https://doi.org/10.1016/j.onano.2022.100066
Sousa, S., Ramos, A., Evtuguin, D. V., & Gamelas, J. A. F. (2016). Xylan and xylan derivatives—Their performance in bio-based films and effect of glycerol addition. *Industrial Crops and Products, 94*, 682-689. https://doi.org/https://doi.org/10.1016/j.indcrop.2016.09.031
Sun, X., Wang, J., Zhang, H., Dong, M., Li, L., Jia, P., . . . Wang, L. (2021). Development of functional gelatin-based composite films incorporating oil-in-water lavender essential oil nano-emulsions: Effects on physicochemical properties and cherry tomatoes preservation. *LWT, 142*, 110987. https://doi.org/https://doi.org/10.1016/j.lwt.2021.110987
Tavassoli, M., Sani, M. A., Khezerlou, A., Ehsani, A., & McClements, D. J. (2021). Multifunctional nanocomposite active packaging materials: Immobilization of quercetin, lactoferrin, and chitosan nanofiber particles in gelatin films. *Food Hydrocolloids, 118*, 106747. https://doi.org/https://doi.org/10.1016/j.foodhyd.2021.106747
Wang, H., Xue, T., Wang, S., Jia, X., Cao, S., Niu, B., . . . Yan, H. (2022). Preparation, characterization and food packaging application of nano ZnO@Xylan/quaternized xylan/polyvinyl alcohol composite films. *International Journal of Biological Macromolecules, 215*, 635-645. https://doi.org/https://doi.org/10.1016/j.ijbiomac.2022.06.157
Wang, S., Ren, J., Kong, W., Gao, C., Liu, C., Peng, F., & Sun, R. (2014). Influence of urea and glycerol on functional properties of biodegradable PVA/xylan composite films. *Cellulose, 21*(1), 495-505. https://doi.org/10.1007/s10570-013-0091-4
Wang, Y., Guo, X., Li, J., Jia, W., Qian, F., Wang, H., & Lv, Y. (2021). Synergistic effects of (3-mercaptopropyl)trimethoxysilane and citric acid on the improvement of water vapor barrier performance of polyvinyl alcohol/xylan packaging films. *Industrial Crops and Products, 171*, 113822. https://doi.org/https://doi.org/10.1016/j.indcrop.2021.113822
Wu, H., Wang, J., Li, T., Lei, Y., Peng, L., Chang, J., . . . Zhang, Z. (2023). Effects of cinnamon essential oil-loaded Pickering emulsion on the structure, properties and application of chayote tuber starch-based composite films. *International*

Journal of Biological Macromolecules, 240, 124444. https://doi.org/https://doi.org/10.1016/j.ijbiomac.2023.124444

Xu, T., Gao, C., Feng, X., Huang, M., Yang, Y., Shen, X., & Tang, X. (2019). Cinnamon and clove essential oils to improve physical, thermal and antimicrobial properties of chitosan-gum arabic polyelectrolyte complexed films. *Carbohydrate Polymers, 217*, 116-125. https://doi.org/https://doi.org/10.1016/j.carbpol.2019.03.084

Yang, Q., Zheng, F., Chai, Q., Li, Z., Zhao, H., Zhang, J., . . . Cui, B. (2024). Effect of emulsifiers on the properties of corn starch films incorporated with *Zanthoxylum bungeanum* essential oil. *International Journal of Biological Macromolecules, 256*, 128382. https://doi.org/https://doi.org/10.1016/j.ijbiomac.2023.128382

Ye, Z.-H., & Zhong, R. (2022). Outstanding questions on xylan biosynthesis. *Plant Science, 325*, 111476. https://doi.org/https://doi.org/10.1016/j.plantsci.2022.111476

Zhang, B., Liu, Y., Peng, H., Lin, Y., & Cai, K. (2023a). Effects of ginger essential oil on physicochemical and structural properties of agar-sodium alginate bilayer film and its application to beef refrigeration. *Meat Science, 198*, 109051. https://doi.org/https://doi.org/10.1016/j.meatsci.2022.109051

Zhang, D., Cao, G., Bu, N., Huang, L., Lin, H., Mu, R., . . . Wang, L. (2023b). Multi-functional konjac glucomannan/chitosan bilayer films reinforced with oregano essential oil loaded β-cyclodextrin and anthocyanins for cheese preservation. *International Journal of Biological Macromolecules, 244*, 125365. https://doi.org/https://doi.org/10.1016/j.ijbiomac.2023.125365

Zhang, M., Li, Q., Qi, H., & Xiang, Z. (2024). Significantly improve film formability of acetylated xylans by structure optimization and solvent screening. *International Journal of Biological Macromolecules, 256*, 128523. https://doi.org/https://doi.org/10.1016/j.ijbiomac.2023.128523

Zhang, Q., Zhang, C., Luo, X., Wang, Z., Guo, J., & Bi, Y. (2022). Protein stabilized seabuckthorn fruit oil Nanoemulsion：Preparation, characterization and performance research. *Food Bioscience, 46*, 101597. https://doi.org/https://doi.org/10.1016/j.fbio.2022.101597

Zhang, S., Cheng, X., Fu, Q., Li, Y., Wu, P., Qiao, Y., . . . Ai, S. (2023c). Pectin-nanolignin composite films with water resistance, UV resistance, and antibacterial activity. *Food Hydrocolloids, 143*, 108783. https://doi.org/https://doi.org/10.1016/j.foodhyd.2023.108783

Zhang, X., Liu, D., Jin, T. Z., Chen, W., He, Q., Zou, Z., . . . Guo, M. (2021). Preparation and characterization of gellan gum-chitosan polyelectrolyte complex films with the incorporation of thyme essential oil nanoemulsion. *Food Hydrocolloids, 114*, 106570. https://doi.org/https://doi.org/10.1016/j.foodhyd.2020.106570

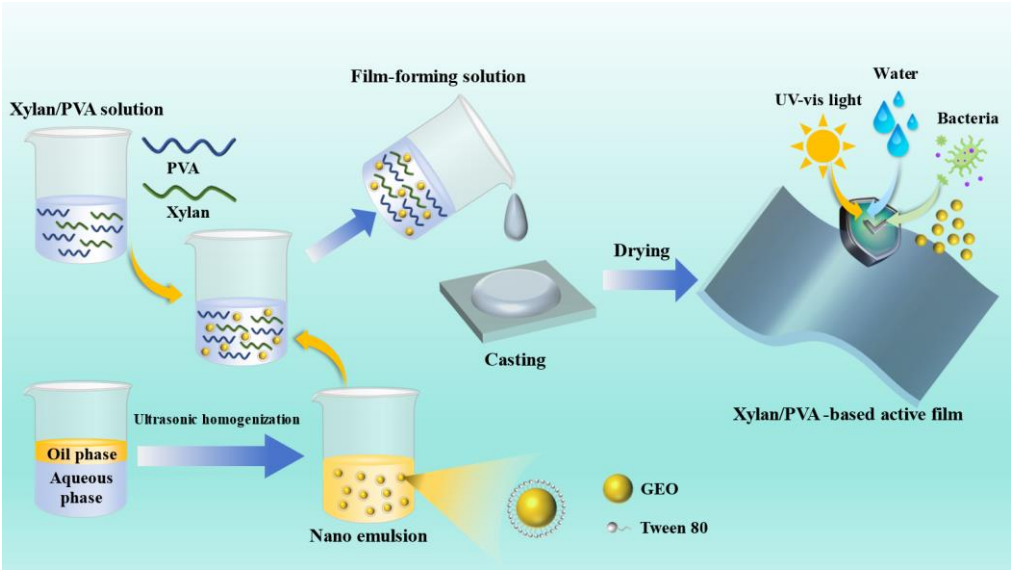

Fig. 1. Schematic illustration of the preparation of xylan/PVA-based active films.

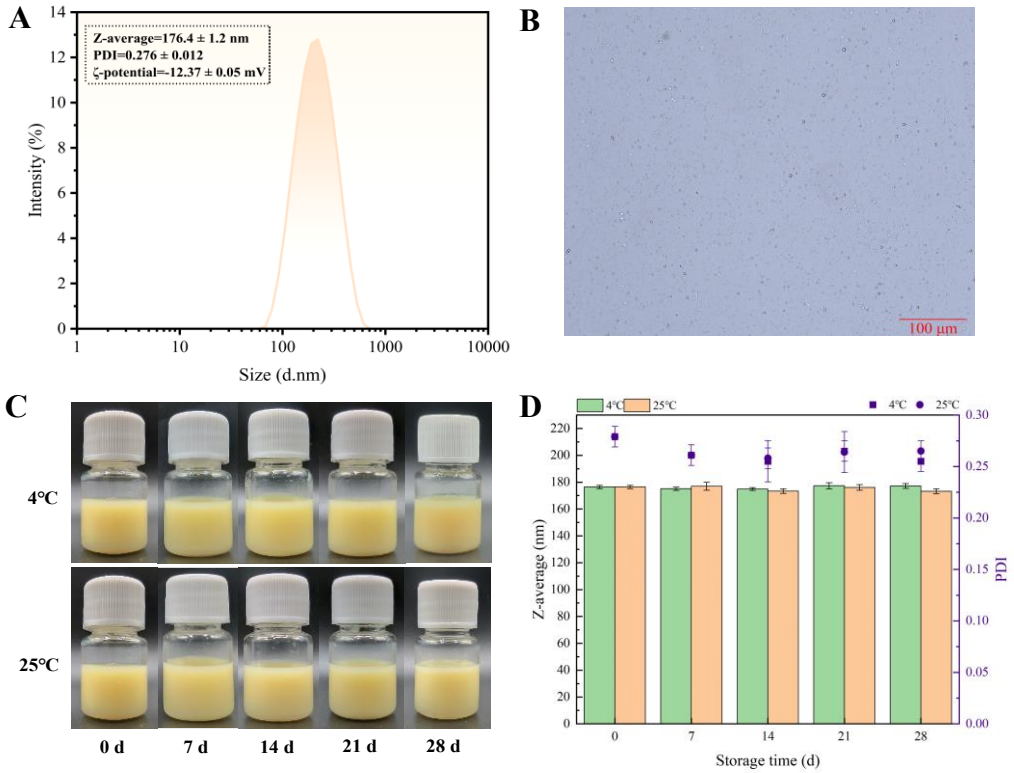

Fig. 2. Particle size distribution, zeta-potential and PDI of GEO-NEs (A), microscopy images of GEO-NEs (B), and changes in appearance, average particle size, and PDI of GEO-NEs during 0~28 d.

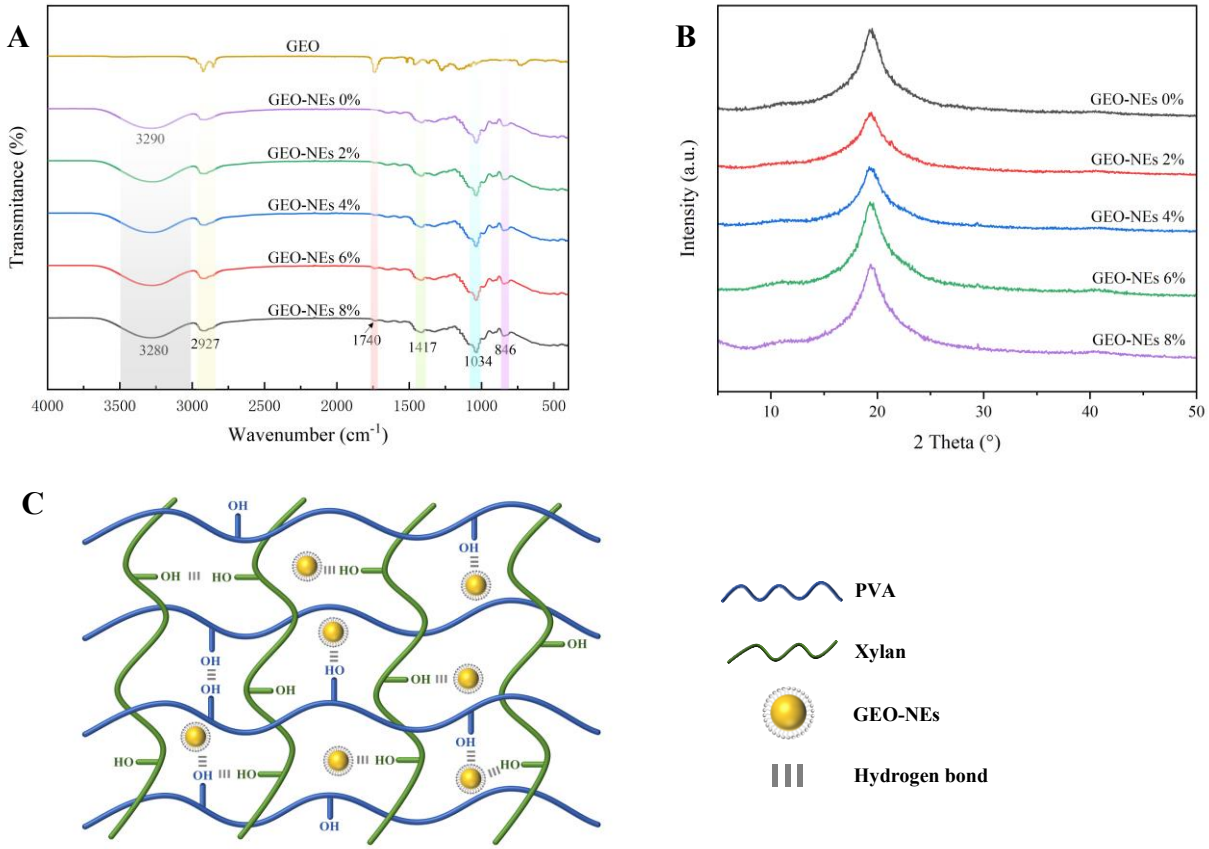

Fig. 3. FT-IR spectra (A), X-ray diffraction spectra (B) of xylan/PVA films containing different concentrations of GEO-NEs and schematic illustration of hydrogen bonding interactions in the film matrix (C).

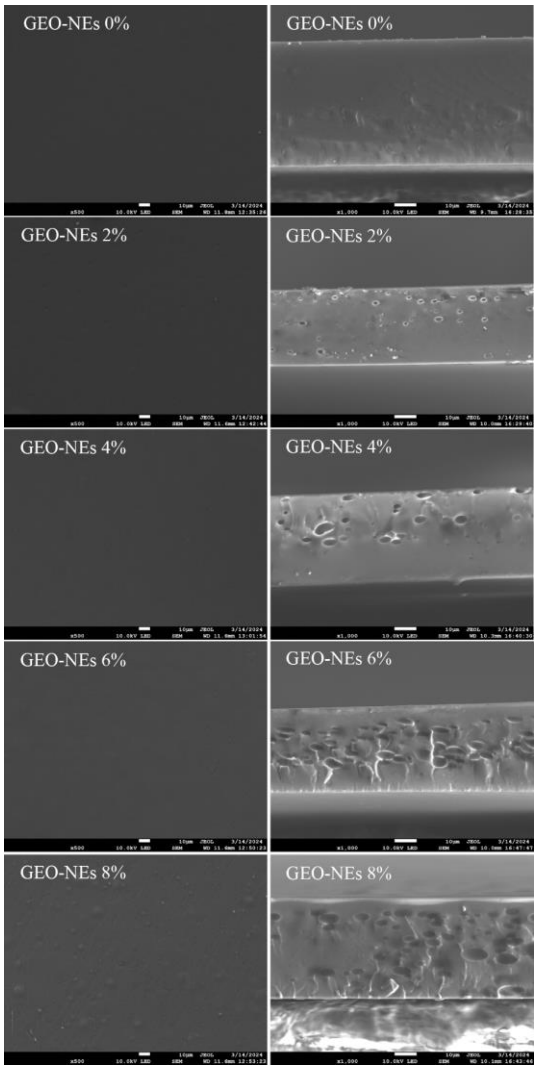

Fig. 4. SEM micrographs of the surfaces (left column) and the cross-sections (right column) of xylan/PVA films containing different concentrations of GEO-NEs.

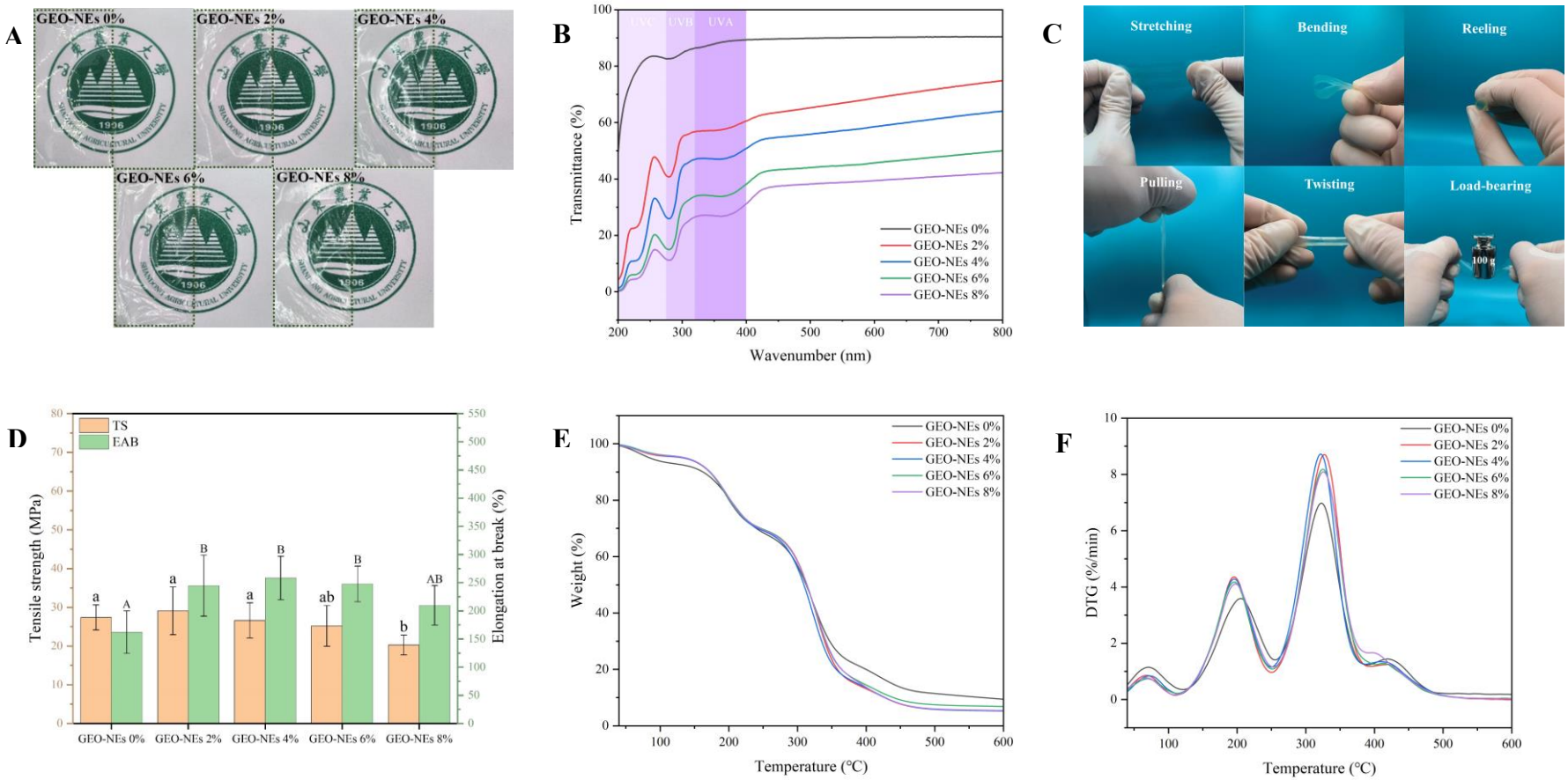

Fig. 5. Digital photographs (A), UV transmittance (B), various deformations (C), tensile strength and elongation at break (D), TGA (A) and DTG (B) thermograms of xylan/PVA films containing different concentrations of GEO-NE.

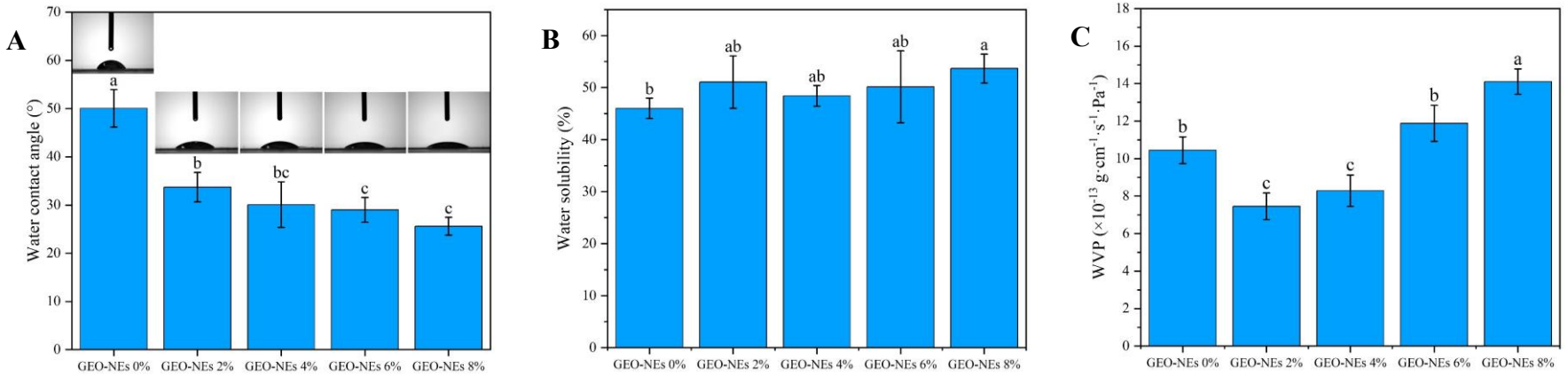

Fig. 6. WCA (A), WS (B) and WVP (C) of xylan/PVA films containing different concentrations of GEO-NEs.

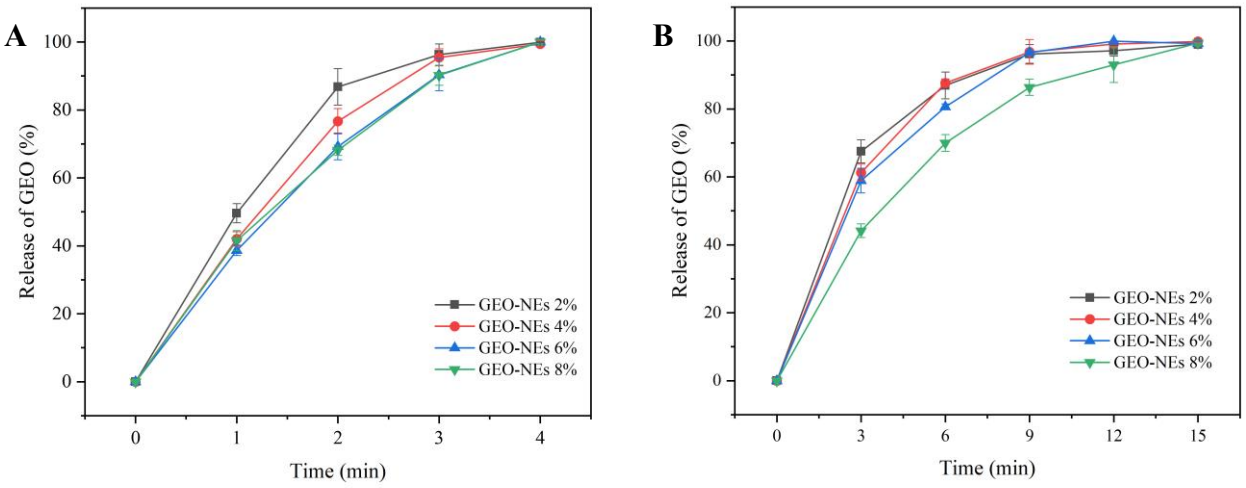

Fig. 7. Release of GEO from films in 10 % ethanol (A) and 90 % ethanol (B).

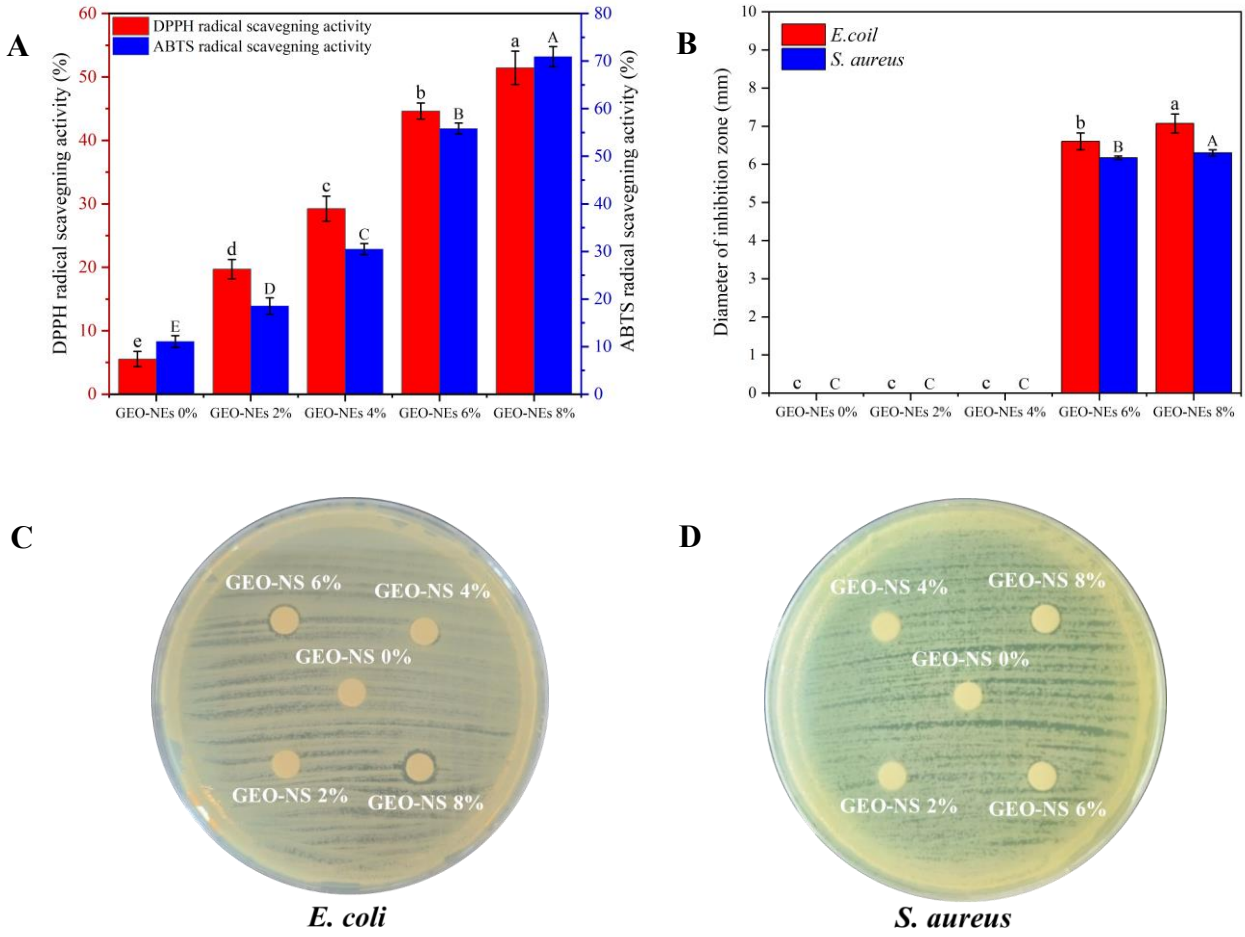

Fig. 8. Antioxidant activity (A), inhibition zones (B) and antibacterial pictures (C, D) of xylan/PVA films containing different concentrations of GEO-NEs.

Supplementary material

Table S1 The color parameters and opacity of films.

	L*	a*	b*	△E	Opacity
GEO-NEs 0%	92.72±0.03^{a}	1.08±0.03^{a}	0.76±0.08^{e}	0.15±0.06^{e}	0.84±0.07^{c}
GEO-NEs 2%	92.17±0.11^{b}	0.89±0.06^{b}	1.65±0.18^{d}	1.16±0.19^{d}	3.05±0.14^{b}
GEO-NEs 4%	92.01±0.29^{b}	0.83±0.05^{bc}	2.00±0.05^{c}	1.55±0.19^{c}	3.89±0.11^{ab}
GEO-NEs 6%	91.94±0.10^{b}	0.78±0.08^{c}	2.38±0.16^{b}	1.93±0.17^{b}	5.07±0.64^{a}
GEO-NEs 8%	91.53±0.25^{c}	0.65±0.05^{d}	2.95±0.31^{a}	2.63±0.39^{a}	5.47±1.45^{a}

Note: Different letters in the same column indicate significant differences ($P < 0.05$).